

RESEARCH ARTICLE

# Parametric generation and phase locking of multiple sidebands in the regime of full-back-conversion

Wenhao Wang<sup>1</sup>, Yudong Tao<sup>1</sup>, Jingui Ma<sup>1</sup>, Jing Wang<sup>1</sup>, Peng Yuan<sup>1</sup>, Dongfang Zhang<sup>1</sup>, and Liejia Qian<sup>1,2</sup>

<sup>1</sup>School of Physics and Astronomy, Shanghai Jiao Tong University, Shanghai, China

<sup>2</sup>Tsung-Dao Lee Institute, Shanghai Jiao Tong University, Shanghai, China

(Received 14 November 2022; revised 26 January 2023; accepted 13 February 2023)

## Abstract

Parametric interaction allows both forward and backward energy transfers among the three interacting waves. The back-conversion effect is usually detrimental when unidirectional energy transfer is desired. In this theoretical work, we manifest that the back-conversion effect underpins the direct generation of the picosecond pulse train without the need for a laser resonator. The research scenario is an optical parametric amplification (OPA) that consists of a second-order nonlinear medium, a quasi-continuous pump laser and a sinusoidal amplitude-modulated seed signal. The back-conversion of OPA can transfer the modulation peaks (valleys) of the incident signal into output valleys (peaks), which inherently induces spectral sidebands. The generation of each sideband is naturally accompanied with a phase shift of  $\pm\pi$ . In the regime of full-back-conversion, the amount and amplitude of the sidebands reach the maximum simultaneously, and their phase constitutes an arithmetic sequence, leading to the production of a picosecond pulse train. The generated picosecond pulse train can have an ultrahigh repetition rate of 40 GHz or higher, which may facilitate ultrafast applications with ultrahigh speed.

**Keywords:** picosecond pulse train; quadratic parametric process; sideband generation

## 1. Introduction

An optical modulator controls the light amplitude or phase through the effects of electro-optics, acoustic-optics, thermooptics or optico-optics<sup>[1–6]</sup>. Optical modulators have been vital in optical signal processors, photonic integrated circuits and fiber optic communication networks<sup>[7–9]</sup>. In particular, the combination of an intracavity optical modulator and a laser resonator has been routinely utilized for generating mode-locked lasers or optical frequency combs<sup>[10–13]</sup>. Intracavity modulation can be achieved by saturable absorption<sup>[14]</sup>,  $\chi^{(2)}$ <sup>[15–18]</sup> or  $\chi^{(3)}$ <sup>[19]</sup> nonlinear processes. Regardless of the type of optical modulator, an optical resonator is indispensable to establish the periodic feedback of gain/loss. It is a nontrivial task to achieve phase locking of many longitudinal modes and generate mode-locked lasers without a laser resonator.

In this paper, we propose a novel category of optical modulator based on the  $\chi^{(2)}$  parametric process, and

theoretically demonstrate that such an optical modulator enables the direct generation and phase locking of multiple sidebands without the need for optical resonators. The optical setup of the proposed optical modulator looks almost the same as an optical parametric amplifier (OPA), which does not require any optical components other than a  $\chi^{(2)}$  medium (Figure 1(a)). However, its transfer function is fundamentally different from OPAs. Conventionally, OPAs are operated in the regime of either small-signal amplification (where pump depletion is negligible) or saturated amplification, wherein back-conversion is carefully avoided<sup>[20]</sup>. In these OPAs, the  $\chi^{(2)}$  parametric process cannot expand the signal bandwidth, and the signal waveform remains almost the same during amplification.

However, in our scheme, the OPAs are deliberately pushed into the regime of full-back-conversion. It is well known that for an amplitude-modulated (AM) seed signal, those modulation peaks with higher amplitude deplete the pump more quickly, so they switch into back-conversion earlier than those modulation valleys. We demonstrate that in the regime of full-back-conversion, the signal waveform  $A_{\text{out}}(t)$  evolves into exactly the reciprocal of the incident waveform  $A_{\text{in}}(t)$ . In other words, OPA acts as an optical modulator that

Correspondence to: Jing Wang and Peng Yuan, School of Physics and Astronomy, Shanghai Jiao Tong University, Shanghai 200240, China. Email: wangj1118@sjtu.edu.cn (J. Wang); pengyuan@sjtu.edu.cn (P. Yuan)

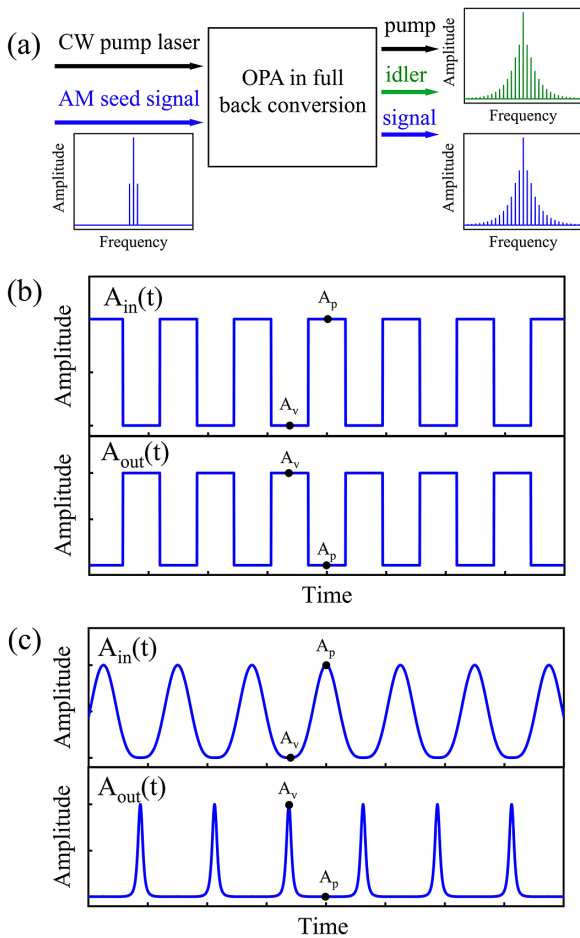


**Figure 1.** (a) Schematic of a  $\chi^{(2)}$ -based optical modulator that provides a reciprocal-type transfer function. It consists of an OPA that is pumped by a quasi-continuous-wave laser and seeded by an amplitude-modulated (AM) laser. The output signal waveforms  $A_{out}(t)$  calculated for (b) a square-modulated seed signal  $A_{in}(t)$  and for (c) a sinusoidal AM seed signal  $A_{in}(t)$ . Here,  $A_p$  and  $A_v$  denote the modulation peak and valley of a sinusoidal AM seed signal.

provides a reciprocal-type transfer function. For a square-modulated seed signal, such a modulator acts as an optical inverter, which changes the ‘1’ amplitude levels into ‘0’, and vice versa (Figure 1(b)). In particular, the reciprocal of a sinusoidal AM waveform is a train of Lorentz-shaped pulses, wherein the pulse duration is significantly shorter than the modulation period of the incident AM waveform. This link promises to produce a picosecond pulse train directly from a sinusoidal AM laser without the need for an optical resonator.

The paper is organized as follows. Section 2 characterizes how the  $\chi^{(2)}$  parametric process enables a reciprocal-type transfer function and how such a transfer function results in sideband generation in the frequency domain, as well as how the phase of all the sidebands evolves, which changes from the disorder state to the phase locking state. Section 3 studies the temporal and spectral characteristics of the output ultrashort pulse train, as well as their dependencies on the

parameters of the OPA and sinusoidal AM. Section 4 discusses the influences of the crystal dispersion and parametric super-fluorescence (PSF). Section 5 presents the conclusion.

## 2. Generation and phase locking of sidebands

To demonstrate the sideband generation and phase locking in the regime of full-back-conversion, we simulate the  $\chi^{(2)}$  parametric process within a periodically poled lithium niobate (PPLN) waveguide by solving the coupled-wave equations<sup>[21]</sup> under the slowly varying envelope approximation, as given by the following:

$$\begin{aligned} \frac{\partial A_s(z,t)}{\partial z} + \sum_{m=1}^{\infty} \frac{(-i)^{m-1}}{m!} k_s^{(m)} \frac{\partial^m A_s(z,t)}{\partial t^m} &= -i \frac{d(z)\omega_s}{n_s c_0} A_p(z,t) A_i^*(z,t) e^{-i\Delta k \cdot z}, \\ \frac{\partial A_i(z,t)}{\partial z} + \sum_{m=1}^{\infty} \frac{(-i)^{m-1}}{m!} k_i^{(m)} \frac{\partial^m A_i(z,t)}{\partial t^m} &= -i \frac{d(z)\omega_i}{n_i c_0} A_p(z,t) A_s^*(z,t) e^{-i\Delta k \cdot z}, \\ \frac{\partial A_p(z,t)}{\partial z} + \sum_{m=1}^{\infty} \frac{(-i)^{m-1}}{m!} k_p^{(m)} \frac{\partial^m A_p(z,t)}{\partial t^m} &= -i \frac{d(z)\omega_p}{n_p c_0} A_s(z,t) A_i(z,t) e^{i\Delta k \cdot z}, \end{aligned} \quad (1)$$

where  $A_{s,i,p}$ ,  $\omega_{s,i,p}$  and  $n_{s,i,p}$  are the complex envelopes, carrier frequency and refractive index of the signal, idler and pump, respectively,  $d(z) = \pm d_{\text{eff}}$  is the nonlinear coupling coefficient of collinear PPLN with collinear geometry, which changes sign in each quasi-phase matching period<sup>[22]</sup>,  $\Delta k = k_p - k_s - k_i$  is the wave-vector mismatch and  $k^{(m)} = \partial^{(m)} k / \partial \omega^{(m)}$  refers to the effects of  $m$ th-order dispersion. In our simulations, the pump laser adopts a 527 nm pulse of 10 ns in duration and  $I_p = 100 \text{ MW/cm}^2$  in intensity, which is below the damage threshold of PPLN<sup>[23]</sup>. The seed signal adopts a sinusoidal AM laser of  $10 \text{ W/cm}^2$ , which contains an initial pair of sidebands at the frequency offset of  $\pm\Omega = \pm 40 \text{ GHz}$  with respect to the center frequency line at  $\lambda_{s0} = 1030 \text{ nm}$ . In the time domain, the seed signal exhibits an amplitude modulation characterized by a modulation frequency of  $\Omega = 40 \text{ GHz}$  and an extinction ratio (ER) of 30 dB. Here, the ER is defined by the intensity ratio between the modulation peak and valley. It is a critical parameter that determines how many sidebands can be produced in our scheme. Nowadays, commercial electric-optic modulators can easily achieve an ER of 30–40 dB<sup>[24]</sup>. Our scheme does not require a carrier-envelope stable phase of the pump and signal pulse. For clarification, the effects of medium dispersion and the super-fluorescence noise are excluded in this section, and will be discussed separately in Section 4.

It is known that in the  $\chi^{(2)}$  parametric process, the temporal shape and duration of the signal change significantly upon back-conversion<sup>[21]</sup>. Since the parametric wave-mixing is instantaneous, each temporal slice of an AM seed signal amplifies independent of the others and thus experiences a different regime of gain saturation. The modulation peaks deplete the pump more quickly than the valleys do. In our simulated case (Figure 2(a)), the modulation peaks maximally deplete the pump at a crystal length of  $L_p = 12.8 \text{ mm}$

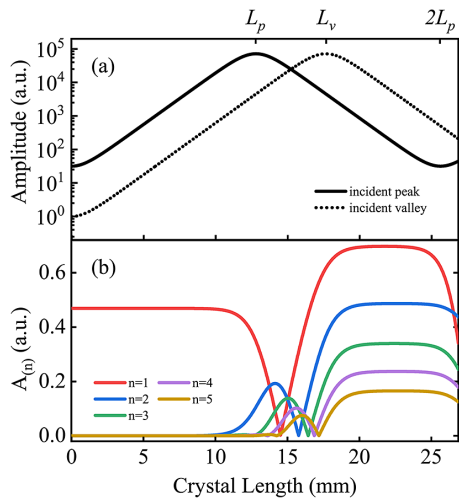


**Figure 2.** (a) Amplitude evolution of the incident modulation peak (solid line) and valley (dotted line) versus the crystal length. (b) Amplitude evolution of the first five orders of sidebands  $A_{(n)}$ , where  $n$  refers to the order for each sideband.

and then fall into back-conversion, while the valleys take a longer crystal length of  $L_v = 17.7$  mm before switching into back-conversion. After a certain crystal length, the amplitude of the incident valleys surpasses that of the incident peaks. This implies that the incident peaks evolve into valleys, while the valleys evolve into peaks.

The initial amplitude ratio between the modulation peaks ( $A_p$ ) and valleys ( $A_v$ ) is determined by the ER as  $A_p/A_v = \sqrt{ER}$ . When the incident peaks (valleys) turn into valleys (peaks), the intensity ratio between the initial peaks and valleys transfers to the reciprocal of the initial value with a crystal length of  $L_v < L < 2L_p$  according to Figure 2(a). For a temporal AM signal, this amplitude relationship indicates that the output waveform of signal  $A_{out}(t)$  would be approximately the reciprocal of the incident signal waveform  $A_{in}(t)$ :

$$A_{out}(t) \approx \frac{a}{A_{in}(t)}, \quad (2)$$

where the coefficient  $a$  represents the amplitude gain of the OPA. We define this regime ( $L_v < L < 2L_p$ ) characterized by such a reciprocal-type transfer function as full-back-conversion.

For a sinusoidal AM seed signal, the spectral counterpart of such a reciprocal-type transfer function is the generation and phase locking of multiple sidebands. Figure 2(b) depicts the amplitude evolution of each order sideband during the whole amplification course. The  $n$ th-order sideband refers to the frequency line that has a frequency interval of  $n\Omega$  with respect to the signal frequency line. The amplitude has been normalized to that of the center frequency line. At the beginning with  $L < L_p$ , there only exists the first-order sidebands ( $n = \pm 1$ ) with a constant amplitude. This regime just corresponds to the amplification regime of conventional

OPAs, where back-conversion does not occur. This explains why OPAs have never been used for sideband generation before our work.

Then at  $L = L_p$  when the modulation peaks of the signal turn into back-conversion, the initial pair of sidebands declines, while the second-order sidebands ( $n = \pm 2$ ) arise. Afterwards, higher-order sidebands gradually arise and quickly grow. We note that in the regime of full-back-conversion ( $L_v < L < 2L_p$ ), both the amount and the amplitude of the sidebands reach the maximum. Although it has been long recognized that the temporal shape of the signal changes significantly upon back-conversion, this is the first time that the back-conversion effect is deliberately exploited for sideband generation.

In general, an OPA experiences the regimes of small-signal amplification, saturated amplification, back-conversion and full-back-conversion in sequence with the increase of crystal length. Figure 3 summarizes the spectral characteristics of the pump, signal and idler in these four regimes, which demonstrates how the multiple sidebands are induced and how the phase of all the induced sidebands evolves into an arithmetic sequence. Essentially, the interacting wave naturally experiences a phase shift of  $\pi$  or  $-\pi$  during its annihilation or creation in parametric processes<sup>[25]</sup>. In the small-signal amplification regime (Figure 3(a)), the pump keeps a single frequency line with an initial phase of  $\varphi_p = 0$ , while the three frequency lines contained by the sinusoidal AM seed signal also have an equal phase of  $\varphi_s = 0$ . They induce an idler wave that spontaneously chooses an initial phase that satisfies  $\varphi_i = \varphi_p - \varphi_s - \pi/2$  to optimize signal amplification<sup>[26]</sup>. So, initially the idler wave has three frequency lines with an equal phase of  $\varphi_i = -\pi/2$ .

Then in the regime of saturated amplification (Figure 3(b)), pump depletion becomes significant. Through the pump depletion, the signal laser imprints its sinusoidal amplitude modulation onto the pump waveform. As a result, the pump acquires a pair of sidebands. The new production of this pair of sidebands is naturally accompanied by a phase shift of  $\pm\pi$  with respect to the initial pump phase. Afterwards, the parametric wave-mixing between the +1st (−1st) sideband of pump and the −1st (+1st) sideband of idler generates the +2nd (−2nd) sideband of signal. This pair of newly induced signal sidebands also spontaneously chooses an optimum phase that satisfies  $\varphi_s = \varphi_p - \varphi_i - \pi/2$ . Hence, the phase of  $\pm 2$ nd sidebands in the signal exhibits a phase shift of  $\pm\pi$  with respect to the initial  $\pm 1$ st sidebands. The presence of  $\pm 2$ nd sidebands in the signal wave then induces the production of  $\pm 2$ nd sidebands in the idler wave. After that, the OPA falls into the back-conversion regime (Figure 3(c)), where laser energy flows back from the signal and idler to the pump. Thus, the amplitude of the signal and idler declines, while the amplitude of the pump reverses to increasing. Nevertheless, the number of sidebands in the pump, signal and idler further increases due

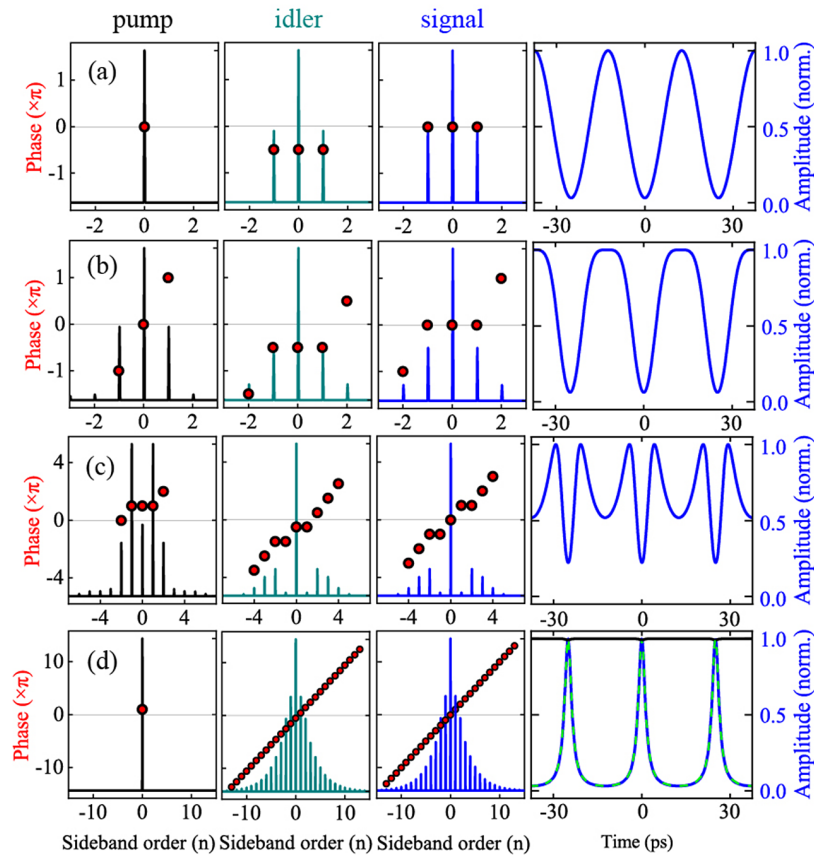


**Figure 3.** (a) The amplitude (vertical lines) and phase (red circles) of each sideband for the pump, idler and signal calculated at various crystal lengths of (a)  $L = 0$ , (b)  $L = L_p = 12.8$  mm, (c)  $L = 14.5$  mm and (d)  $L = 21.5$  mm. The right-hand column presents the corresponding waveforms of the signal (blue solid line), pump (black solid line) and idler (green dashed line).

to further parametric mixing of multiple frequency lines. The regime of back-conversion leads to the nonlinear production of all the sidebands. In particular, in Figure 3(c) the  $\pm 1$ st sidebands bounce into reproduction after an entire back-conversion, and this reproduction is accompanied by an extra phase shift of  $\pm\pi$ . As a result, the  $\pm 1$ st sidebands of the signal now have the same phase as the  $\pm 2$ nd sidebands.

Finally, the full-back-conversion regime is characterized by the phenomena that the number of signal sidebands reaches the maximum, and all the sidebands bounce into reproduction after experiencing an entire back-conversion. On the one hand, since the reproduction of each sideband is accompanied by a phase shift of  $\pm\pi$ , the phase of all the sidebands constitutes an arithmetic sequence in this regime (Figure 3(d)). The temporal counterpart of such a frequency comb can be thus qualitatively evaluated as follows:

$$\begin{aligned}
 E(t) &= E_0 \exp(i\omega_0 t) \sum_{n=-N}^N \exp[in(\pi + \Omega t)] \\
 &= E_0 \exp(i\omega_0 t) \frac{\cos\left(\frac{2N+1}{2}\Omega t\right)}{\cos\left(\frac{\Omega t}{2}\right)}, \quad (3)
 \end{aligned}$$

where  $\omega_0$  is the center frequency of signal and  $2N$  refers to the number of sidebands. This result signifies that an

ultrashort pulse train has been generated. On the other hand, since all the sidebands have experienced an entire back-conversion, almost all the energy flows back to the pump, such that the pump depletion becomes negligible and the pump almost recovers to a single frequency line, just as in the small-signal amplification regime. In the right-hand column of Figure 3(d), we present the temporal waveform of the output pump, idler and signal in this regime, where the amplitude modulation on the pump laser (black line) becomes negligible and the output signal waveform exhibits an ultrashort pulse train. Except for the signal wave, an idler wave with the same number of sidebands is also generated.

### 3. Characterization of the ultrashort pulse train

In the full-back-conversion regime, numerical simulations show that the amplitude of the output signal is inversely proportional to the incident amplitude (Figure 4(a)). Consequently, the output signal waveform  $A_{\text{out}}(t)$  fits well with the reciprocal of the incident signal waveform. With such a transfer function, a sinusoidal AM seed signal single pulse with a temporal amplitude as given by

$$A_{\text{in}}(t) = \frac{A_p + A_v}{2} + \frac{A_p - A_v}{2} \sin\left(\Omega t - \frac{\pi}{2}\right) \quad (4)$$

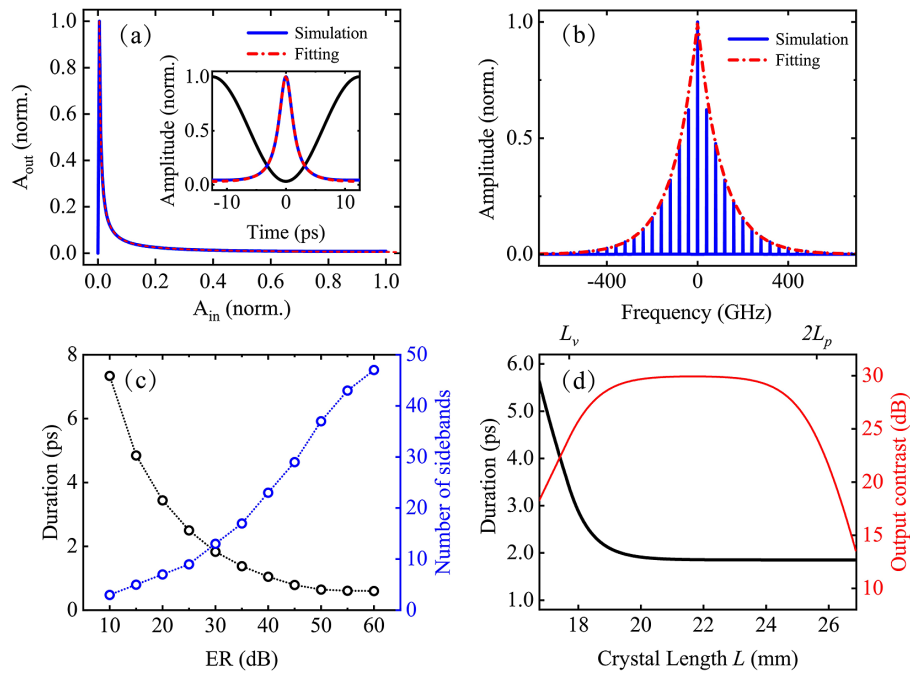


**Figure 4.** (a) The output signal amplitude  $A_{\text{out}}$  versus incident signal amplitude  $A_{\text{in}}$  (blue), which agrees well with a reciprocal-type transfer function (red). The inset plots the incident (black) and output signal waveform calculated by numerical simulation (blue) and Equation (5) (red). (b) The spectrum of the output signal (blue) and the fitting based on Equation (10). (c) The number of sidebands (with the relative amplitude  $\geq 0.1$ ) and the temporal duration of the output signal against the change of ER. (d) Stability of the output pulse duration and temporal contrast against the change of crystal length.

evolves into the following:

$$A_{\text{out}}(t) = \frac{a}{\frac{A_p + A_v}{2} + \frac{A_p - A_v}{2} \sin\left(\Omega t - \frac{\pi}{2}\right)}, \quad (5)$$

where the coefficient  $a$  links with the amplitude of the output signal, and is related with the saturated gain provided by the  $\chi^{(2)}$  parametric process. With a saturated gain of  $g$ , then the coefficient can be simply expressed by  $a = g(A_v)^2$ . In Equation (4),  $t = 0$  corresponds to a valley of the incident signal, while in Equation (5), the point of  $t = 0$  becomes a modulation peak. Around  $t = 0$ , Equation (5) can be approximated into the following:

$$A_{\text{out}}(t) \approx \frac{4a/A_p}{(\Omega t)^2 + 4A_v/A_p}. \quad (6)$$

Note that such a waveform is highly coincident with that of a Lorentz-shaped pulse, as follows:

$$A_{\text{LZ}}(t) = \frac{1}{\pi} \cdot \frac{\Gamma}{t^2 + \Gamma^2}. \quad (7)$$

Thereby, the temporal duration of the output pulse is dominated by the parameter  $\Gamma$ , which in our case is equal to the following:

$$\Gamma = \sqrt{\frac{4A_v}{\Omega^2 A_p}} = \frac{2}{\Omega \sqrt{ER}}. \quad (8)$$

The pulse duration at half magnitude can thus be solved as follows:

$$T = 2\sqrt{\sqrt{2} - 1}\Gamma \approx 1.29\Gamma. \quad (9)$$

The output pulse duration is proportional to the parameter  $\Gamma$ , which is inversely proportional to the modulation frequency  $\Omega$  as well as the fourth root of the ER of the incident sinusoidal AM signal ( $A_p/A_v = \sqrt{ER}$ ). The limit of the output pulse duration can be estimated using Equations (8) and (9). For such a Lorentz-shaped output pulse, the spectrum can be approximately given by the following:

$$a_{\text{LZ}}(\omega) = e^{-\Gamma|\omega|}. \quad (10)$$

Figure 4(b) shows the spectral amplitude of the output pulse, wherein the blue solid line presents the result obtained for numerical simulation, while the red dashed line depicts the approximate solution calculated based on Equation (10). The spectrum exhibits exponential decay in the leading and trailing wings. The good agreement between the numerical simulation results with Equations (7) and (10) verifies that an OPA operating in the full-back-conversion regime can translate a sinusoidal AM laser into a train of Lorentz-shaped pulses.

A sinusoidal AM seed signal with higher ER induces a train of pulses with shorter duration. As shown in Figure 4(c), an ER of 30 dB leads to the generation of 12 side-

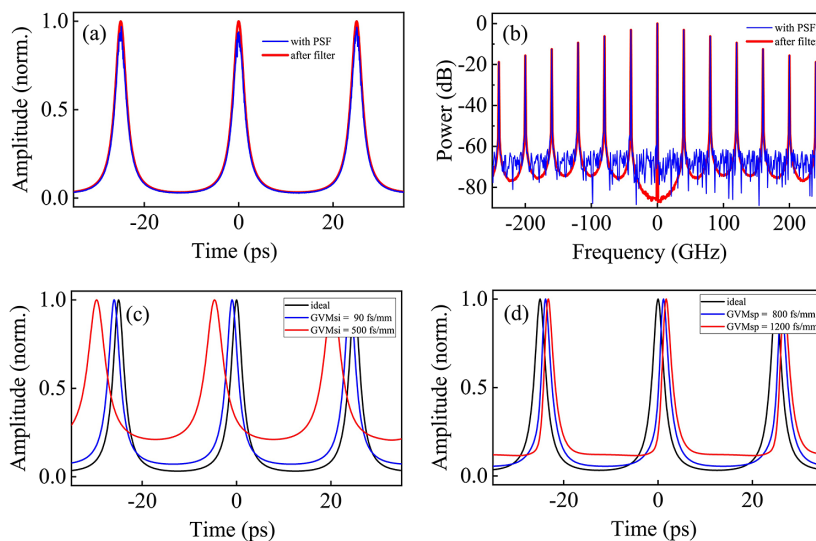


**Figure 5.** (a) Temporal waveform and (b) power spectral density of the output pulse train calculated in the presence of PSF without (blue) and with bandpass filtering (red), respectively. Temporal waveform of the output pulse train calculated for (c)  $GVM_{si} = 0$  (black), 90 fs/mm (blue), 500 fs/mm (red) and (d)  $GVM_{sp} = 0$  (black), 800 fs/mm (blue), 1200 fs/mm (red). Other simulation parameters are set the same as in Figures 3(d) and 4(a).

bands, while an ER of 50 dB leads to 36 sidebands in our simulated case. The former corresponds to a temporal pulse duration of 1.8 ps, while the latter corresponds to 0.6 ps. The temporal duration and the contrast of the output pulses are stable within the whole regime of full-back-conversion (i.e., the crystal length range of 19–25 mm), as indicated by Figure 4(d). In addition, the proposed scheme not only transforms a sinusoidal AM seed signal into a picosecond pulse train, but also amplifies the signal in amplitude. In our case, the output pulse amplitude around  $t = 0$  has a saturated gain of approximately  $10^4$ . This means that the output pulse intensity is approximately  $10^5$  times stronger than the peak intensity of the AM seed signal.

#### 4. Practical consideration

OPAs inherently suffer from the PSF noise<sup>[27]</sup>. Next we identify the effect of PSF on the generation of the picosecond pulse train. A zero-mean stochastic phasor with an uncorrelated Gaussian distribution is introduced into the initial signal wave to mimic the spontaneous parametric down-conversion noise<sup>[28,29]</sup>. The initial energy of the noise field is assumed to be 40 aJ, as given in Ref. [28]. The simulation results show that the presence of PSF does imprint some stochastic amplitude noise onto the output pulse train (Figure 5(a)). However, it has a negligible influence on both the temporal shape and duration of the output pulses. Given that the PSF noise has a bandwidth much wider than the picosecond pulse train, it can be feasibly removed by a bandpass filter. The red lines in Figures 5(a) and 5(b) depict the temporal and spectral amplitude of the output picosecond pulse after bandpass filtering, respectively, which indicates that the influence of PSF has been overcome.

Finally, we study the influence of the medium dispersion. In the context of generating a picosecond pulse train (corresponding to a spectral bandwidth of less than 1 THz), only the first-order dispersion, that is, the group-velocity mismatch (GVM), needs to be considered. In general, the GVM between the interacting waves can cause a temporal shift of the output pulse train. This temporal shift will degrade the  $A_p/A_v$  ratio in Equation (6), which thus has the probability to degrade the temporal duration and contrast of the output picosecond pulse train. For the GVM between the signal and idler wave ( $GVM_{si}$ ), numerical simulations reveal that as long as the overall temporal shift caused by  $GVM_{si}$  is less than the output pulse duration, its influence is negligible. The above simulations, under the assumption of zero GVM, result in an output pulse duration of 1.8 ps (Figure 4(a)). Given that a crystal length of  $L \geq 20$  mm is required for full-back-conversion, the critical value for  $GVM_{si}$  is approximately 90 fs/mm. Figure 5(c) plots the output pulse train calculated with  $GVM_{si} = 90$  fs/mm, which exhibits only a temporal shift relative to the ideal condition with  $GVM_{si} = 0$ . The duration and contrast of each pulse are nearly unchanged. When we purposely increase  $GVM_{si}$  to 500 fs/mm, the pulse duration increases from 1.8 to 3.3 ps, and the pulse contrast dramatically degrades from 30 to 13.5 dB. Practically, the  $GVM_{si}$  in PPLN crystal is only 20 fs/mm, which is much less than the critical value of 90 fs/mm, indicating that the influence of  $GVM_{si}$  is negligible.

Since the pump laser is initially a quasi-continuous-wave, the effect of the GVM between the pump and signal ( $GVM_{sp}$ ) is much less important compared with  $GVM_{si}$ . In our simulated case,  $GVM_{sp} (= 800$  fs/mm) only causes a very small temporal shift of the output pulse train, as shown in Figure 5(d). Even when we increase  $GVM_{sp}$  to 1200 fs/mm

purposely, the duration of each pulse does not change, and only the pulse contrast falls into degradation.

The above practical considerations show that the production of an ultrashort pulse train from parametric wave-mixing prefers a sinusoidal AM seed signal with a high ER and a nonlinear medium with small dispersion  $GVM_{si}$  and high nonlinear coefficient  $d_{eff}$ . A high  $d_{eff}$  is desirable because large nonlinear length (proportional to  $d_{eff}$  as well as the crystal length  $L$ ) is indispensable to transfer an AM signal of high ER into the full-back-conversion regime. If a nonlinear medium with small  $d_{eff}$  is used, a large crystal length becomes necessary to reach full-back-conversion, which increases the PSF as well as the temporal walk off between the signal and idler, thereby degrading the temporal contrast of the output ultrashort pulse train.

## 5. Conclusion

In conclusion, we propose a  $\chi^{(2)}$ -based optical modulator that provides a reciprocal-type transfer function, and further demonstrate that such an optical modulator can directly transfer a sinusoidal AM laser into a train of Lorentz-shaped picosecond pulses, without the need for optical resonators. Being different from conventional  $\chi^{(2)}$  parametric processes, the back-conversion effect that is carefully avoided in previous applications is exploited in our scheme. It is the strong nonlinearity inherent to back-conversion that induces multiple sideband generation and finally enables a reciprocal-type transfer function. Meanwhile, the inherent phase shift of  $\pi$  that accompanies photon annihilation or creation in parametric processes plays an important role in driving all the induced sidebands into phase locking.

Compared to traditional mode-locking techniques, our proposed scheme for producing ultrashort pulse train does not require optical resonators. Thus, it does not require complex alignment and promises a higher pulse repetition rate. The repetition rate of the output picosecond pulse train is exactly equal to the modulation frequency of the AM seed signal. It has been reported that a sinusoidal AM signal with a modulation frequency of THz can be produced by the optical beat between two narrow frequency lines<sup>[30]</sup>. The combination of such a THz modulation and our proposed scheme promises the generation of an ultrashort pulse train with a repetition rate as high as THz, which is impossible by mode-locked laser techniques so far. Another difference is the temporal and spectral characteristics of the output pulses. The pulses produced by our proposed scheme are Lorentz-shaped in the time domain, and the frequency combs contained in the spectrum exhibit exponential decay in two wings. The phase of all the frequency combs constitutes an arithmetic sequence with a phase shift of  $\pi$  between adjacent combs.

Such a high-speed ultrashort pulse train has implications for the efficient generation of multi-cycle THz waves<sup>[31]</sup>.

Previously, THz modulations were produced by optical beating among multiple frequency lines or chirped pulses with various delays<sup>[32–34]</sup>, which were not so stable and difficult to adjust. By comparison, our scheme only requires one single-stage OPA, and thus is much more compact, stable and tunable. In addition, the generation of a picosecond pulse train at signal wavelength is naturally accompanied by the production of another picosecond pulse train at idler wavelength. This implies the potential to directly produce a powerful picosecond pulse train at THz repetition rate in the mid-infrared spectral range.

## Acknowledgement

This work was supported by the National Natural Science Foundation of China (Nos. 61727820, 61905142, 61975120, and 91850203).

## References

1. T. Kobayashi, T. Sueta, Y. Cho, and Y. Matsuo, *Appl. Phys. Lett.* **21**, 341 (1972).
2. M. Kourogi, K. Nakagawa, and M. Ohtsu, *IEEE J. Quantum Electron.* **29**, 2693 (1993).
3. J. Liu, M. Beals, A. Pomerene, S. Bernardis, R. Sun, J. Cheng, L. C. Kimmerling, and J. Michel, *Nat. Photonics* **2**, 433 (2008).
4. K. Yang, S. Zhao, G. Li, and H. Zhao, *Opt. Laser Technol.* **37**, 381 (2005).
5. N. C. Harris, Y. Ma, J. Mower, T. Baehr-Jones, D. Englund, M. Hochberg, and C. Galland, *Opt. Express* **22**, 10487 (2014).
6. T. T. Alkeskjold, J. Lægsgaard, A. Bjarklev, D. S. Hermann, A. Anawati, J. Broeng, J. Li, and S.-T. Wu, *Opt. Express* **12**, 5857 (2004).
7. C. Wang, M. Zhang, X. Chen, M. Bertrand, A. Shams-Ansari, S. Chandrasekhar, P. Winzer, and M. Lončar, *Nature* **562**, 101 (2018).
8. D. A. B. Miller, *J. Lightwave Technol.* **35**, 346 (2017).
9. A. Delmade, M. Krstić, C. Browning, J. Crnjanski, D. Gvozdić, and L. Barry, *Opt. Express* **27**, 24135 (2019).
10. H. D. Lee, G. H. Kim, J. G. Shin, B. Lee, C.-S. Kim, and T. J. Eom, *Sci. Rep.* **8**, 17660 (2018).
11. J. Yao, J. Yao, Y. Wang, S. C. Tjin, Y. Zhou, Y. L. Lam, J. Liu, and C. Lu, *Opt. Commun.* **191**, 341 (2001).
12. K. Yin, B. Zhang, B. Yang, H. Chen, S. Chen, and J. Hou, *Opt. Lett.* **39**, 4259 (2014).
13. S. A. Diddams, L.-S. Ma, J. Ye, and J. L. Hall, *Opt. Lett.* **24**, 1747 (1999).
14. E. J. Saarinen, J. Lyytikäinen, and O. G. Okhotnikov, *Phys. Rev. E* **78**, 016207 (2008).
15. I. Ricciardi, S. Mosca, M. Parisi, F. Leo, T. Hansson, M. Erkintalo, P. Maddaloni, P. De Natale, S. Wabnitz, and M. De Rosa, *Micromachines* **11**, 230 (2020).
16. I. Ricciardi, S. Mosca, M. Parisi, P. Maddaloni, L. Santamaria, P. De Natale, and M. De Rosa, *Phys. Rev. A* **91**, 063839 (2015).
17. J. Khurgin, J.-M. Melkonian, A. Godard, M. Lefebvre, and E. Rosencher, *Opt. Express* **16**, 4804 (2008).
18. J. M. Melkonian, N. Forget, F. Bretenaker, C. Drag, and E. Rosencher, *Opt. Lett.* **32**, 1701 (2007).
19. N. Englebert, C. Mas Arabí, P. Parra-Rivas, S.-P. Gorza, and F. Leo, *Nat. Photonics* **15**, 536 (2021).
20. G. Cerullo, and S. D. Silvestri, *Rev. Sci. Instrum.* **74**, 1 (2003).
21. B. Zhou, J. Ma, J. Wang, P. Yuan, G. Xie, and L. Qian, *Opt. Lett.* **43**, 3790 (2018).

22. O. Gayer, Z. Sacks, E. Galun, and A. Arie, *Appl. Phys. B*, **91**, 343 (2008).
23. <https://www.hcphotonics.com/ppln-guide-materials#6>.
24. <https://www.ixblue.com/photonics-space/intensity-modulators>.
25. N. R. Ian, P. Matousek, H. C. N. Geoffrey, and K. Osvay, *J. Opt. Soc. Am. B* **19**, 2945 (2002).
26. J. Ma, J. Wang, P. Yuan, G. Xie, and L. Qian, *Chin. Opt. Lett.* **15**, 021901 (2017).
27. D. Salerno, S. Minardi, J. Trull, A. Varanavicius, G. Tamosauskas, G. Valiulis, A. Dubietis, D. Caironi, S. Trillo, A. Piskarskas, and P. D. Trapani, *Phys. Rev. Lett.* **91**, 143905 (2003).
28. J. Moses, S.-W. Huang, K.-H. Hong, O. D. Mücke, E. L. Falcão-Filho, A. Benedick, F. Ö. Ilday, A. Dergachev, J. A. Bolger, B. J. Eggleton, and F. X. Kärtner, *Opt. Lett.* **34**, 1639 (2009).
29. J. Wang, J. Ma, Y. Wang, P. Yuan, G. Xie, and L. Qian, *Opt. Lett.* **39**, 2439 (2014).
30. D. N. Schimpf, H. T. Olgun, A. Kalaydzhyan, Y. Hua, N. H. Matlis, and F. X. Kärtner, *Opt. Express* **27**, 11037 (2019).
31. K. Ravi, D. N. Schimpf, and F. X. Kärtner, *Opt. Express* **24**, 25582 (2016).
32. V. Stummer, T. Flöry, G. Krizsán, G. Polónyi, E. Kaksis, A. Pugžlys, J. Hebling, J. A. Fülöp, and A. Baltuška, *Optica* **7**, 1758 (2020).
33. K. L. Vodopyanov, W. C. Hurlbut, and V. G. Kozlov, *Appl. Phys. Lett.* **99**, 041104 (2011).
34. Z. Chen, X. Zhou, C. A. Werley, and K. A. Nelson, *Appl. Phys. Lett.* **99**, 071102 (2011).